Microscale Chaotic Advection Enables Robust Convective DNA Replication

ARTICLE *in* ANALYTICAL CHEMISTRY · OCTOBER 2013

Impact Factor: 5.64 · DOI: 10.1021/ac402611s · Source: PubMed

3 AUTHORS, INCLUDING:

Aashish Priye
Sandia National Laboratories
16 PUBLICATIONS **6** CITATIONS
SEE PROFILE

Y. A. Hassan
Texas A&M University
392 PUBLICATIONS **1,503** CITATIONS
SEE PROFILE

analytical chemistry

Article

pubs.acs.org/ac

Microscale Chaotic Advection Enables Robust Convective DNA Replication

Aashish Priye,[†] Yassin A. Hassan,[‡,§] and Victor M. Ugaz*[,†]

[†]Artie McFerrin Department of Chemical Engineering, [‡]Department of Mechanical Engineering, and [§]Department of Nuclear Engineering, Texas A&M University, College Station, Texas 77843-3122, United States

Supporting Information

ABSTRACT: The ability of chaotic advection under microscale confinement to direct chemical processes along accelerated kinetic pathways has been recognized for some time. However, practical applications have been slow to emerge because optimal results are often counterintuitively achieved in flows that appear to possess undesirably high disorder. Here we present a 3D time-resolved analysis of polymerase chain reaction (PCR)-mediated DNA replication across a broad ensemble of geometric states. The resulting parametric map reveals an unexpectedly wide operating regime where reaction rates remain constant over 2 orders of magnitude of the Rayleigh number, encompassing virtually any realistic PCR condition (temperature, volume, gravitational alignment), a level of robustness previously thought unattainable in the convective format.

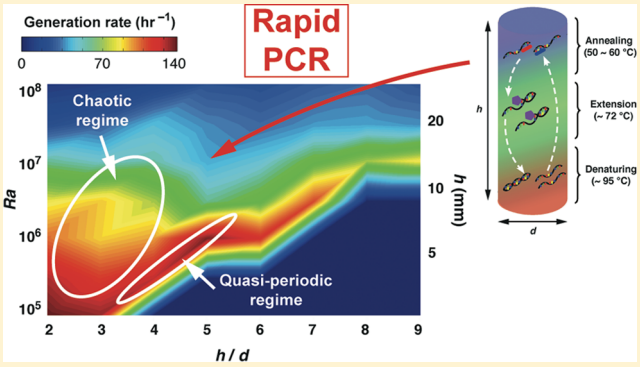

Thermal convection has emerged as a promising approach to enable rapid DNA replication, the polymerase chain reaction (PCR).[1−4] One of the most straightforward implementations of this concept involves harnessing Rayleigh Bénard convection, owing to the inherent simplicity of housing the aqueous reagent mixture in a microliter-scale enclosure (typically cylindrical in shape) heated from below (Figure 1). The interplay between the destabilizing buoyancy force and restoring action of thermal and viscous diffusion in this configuration is expressed in terms of the dimensionless Rayleigh number ($Ra = [g\beta(T_2 - T_1)h^3]/\nu\alpha$; where β is the fluid's thermal expansion coefficient, g is the gravitational acceleration, T_1 and T_2 are the temperatures of the top (cold) and bottom (hot) surfaces, respectively, h is the height of the cylindrical reactor, α is the thermal diffusivity, and ν is the kinematic viscosity). This quantity, coupled with the geometric parameter h/d (d is the reactor diameter), completely specifies the available flow states.[3] The convective arrangement confers an operational advantage because thermocycling is actuated pseudoisothermally by maintaining a gradient between opposing fixed-temperature surfaces, in contrast to conventional designs where the entire bulk volume must be repeatedly heated and cooled. However, this outward simplicity is deceiving because the internal flow fields generated under PCR conditions are not the closed 2D circulatory trajectories conventionally assumed. Instead, the fluid motion displays an unexpectedly rich complexity owing to the onset of chaotic advection in a regime of transition to convective turbulence even though the flow is inertially laminar (characteristic Reynolds numbers ∼30−40). A subset of flow states in this regime are capable of significantly accelerating the reaction, yielding extremely rapid DNA replication rates and a counterintuitive finding that optimal reaction performance occurs under conditions where some of

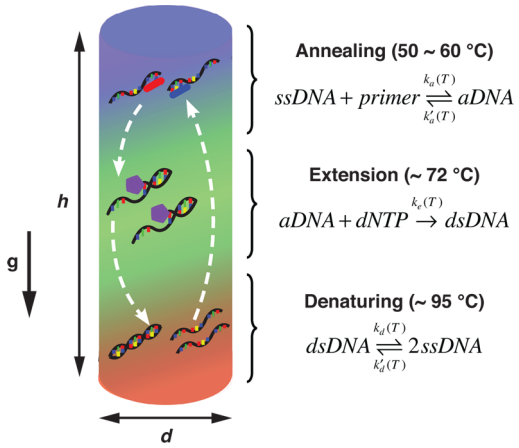

Figure 1. DNA replication via the PCR in a Rayleigh Bénard convection cell. Thermocycling is executed in a cylindrical reactor geometry of height h and diameter d by imposing a temperature gradient between the top and bottom surfaces. A 3-reaction model is depicted whereby a DNA replication cycle occurs as reagents are sequentially transported through temperature zones associated with annealing (top), extension (middle), and denaturing (bottom) processes.

Received: August 14, 2013
Accepted: October 1, 2013
Published: October 1, 2013

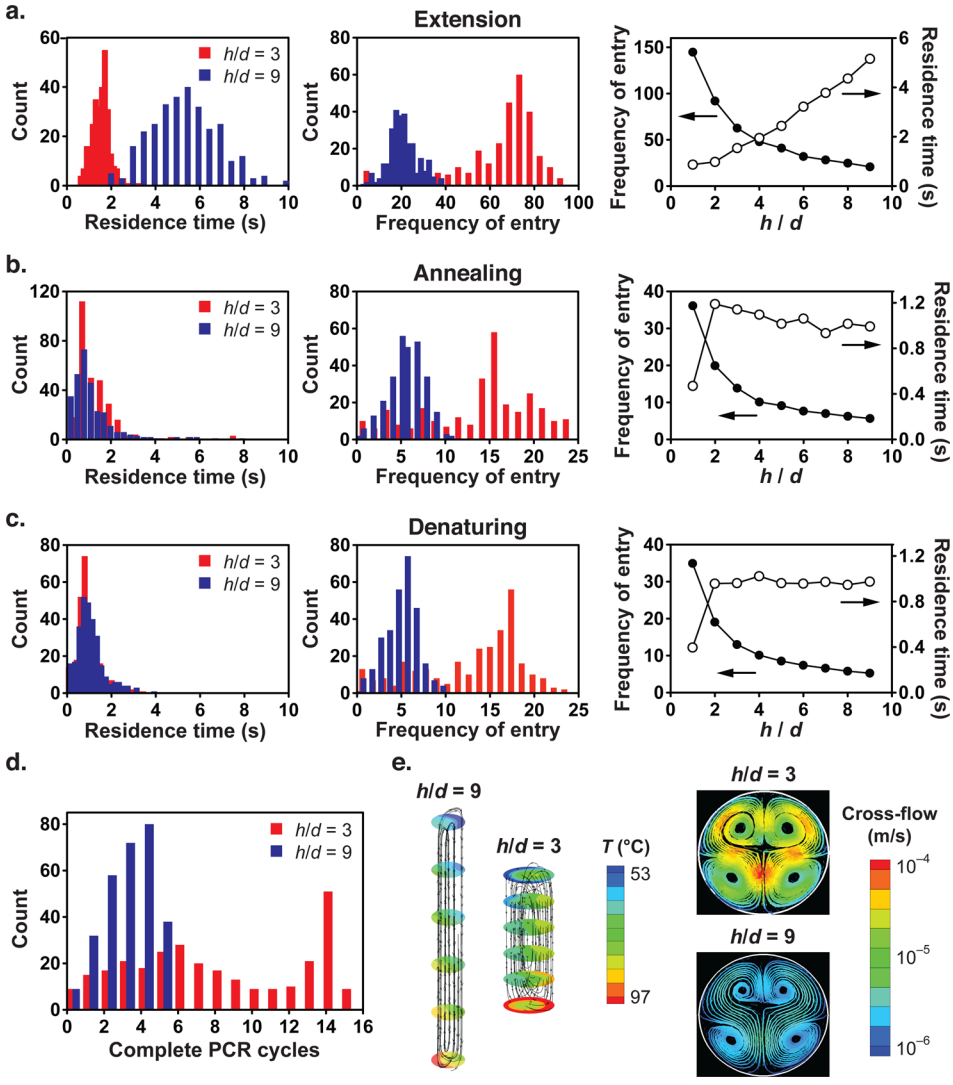

Figure 2. Thermally activated biochemistry is governed by the convective flow field. (a) Laminar flows (h/d = 9) generate longer residence times in the extension temperature zone (left) whereas chaotic flows (h/d = 3) produce a higher frequency of entry (middle), with a gradual transition between extremes at intermediate geometries (right). Both flows yield similar residence times in the (b) annealing and (c) denaturing temperature zones, but the frequency of entry is greater in chaotic flows and the relative trends are maintained across the majority of the geometric parameter space. (d) The number of complete PCR cycles, defined as trajectories sequentially traversing annealing, extension, and denaturing temperature zones, reveal that more complete cycles are executed under chaotic flow conditions. (e) The strengthened chaotic component of the flow at (h/d = 3) is evident by more disordered flow trajectories (left) and a cross-flow component of significantly greater magnitude. Trajectories were obtained from 3D CFD simulations performed over 5 min of convective flow.

the most disordered flows are generated.[3] In this paper, we seek to elucidate the role of chaotic advection and precisely quantify its interplay with the underlying PCR biochemistry throughout the entire 3D reactor volume. These new insights lead to discovery of an incredibly robust operating zone wherein DNA replication rates remain constant over 2 orders of magnitude of *Ra*, encompassing virtually all possible combinations of temperature and reactor volume associated with realistic PCR conditions.

EXPERIMENTAL SECTION

Design and operation of our convective thermocycling instrument has previously been described in detail.[4] Cylindrical reactors were constructed from 0.5 in. diameter polycarbonate rod stock (Amazon Supply) by cutting them to lengths and machining holes to produce reactors with an aspect ratio of h/d = 3 at heights of h = 4.5, 6, and 7.5 mm. PCR experiments were performed to replicate a 237 base pair target from a λ-phage DNA template. A typical 100 μL reaction mixture contained 10 μL of 10× buffer solution, 4 μL of 25 mM $MgCl_2$, 10 μL of dNTPs (2 mM each), 67.8 μL of DI water, 3 μL of each forward and reverse primer, 2 μL of template DNA, and 0.8 μL of KOD polymerase (2.5 units/μL). The enzyme, buffer (buffer no. 1), $MgCl_2$, and dNTPs were supplied with the KOD DNA Polymerase Kit (catalog no. 71085-3; Novagen). Reactors were first rinsed with a 10 mg/mL aqueous solution of bovine serum albumin (catalog no. A2153; Sigma-Aldrich), followed by Rain-X Anti-Fog (SOPUS Products), and dried. We found that these rinsing steps helped minimize adsorption at the sidewalls that may otherwise inhibit the reaction while also enhancing surface wettability so that reagents could be loaded without trapping air pockets inside the reactor. The lower surface of the polycarbonate reactor was sealed using three layers of aluminum tape (catalog no. PCR-AS-200; Axygen, Inc.), after which reagents

dx.doi.org/10.1021/ac402611s | *Anal. Chem.* 2013, 85, 10536−10541

Table 1. Simulated PCR Kinetic Models

step	reaction	T (°C)	rate constant
3-Reaction Model			
denaturing	dsDNA → 2(ssDNA)	92−97	$k_d = 10\ s^{-1}$
annealing	ssDNA + primer → aDNA	55−60	$k_a = 5 \times 10^5\ M^{-1}\ s^{-1}$
extension	aDNA + dNTP → dsDNA	70−74	$k_e = 10^6\ M^{-1}\ s^{-1}$
5-Reaction Model			
renaturing	2(ssDNA) → dsDNA	55−60	$k_d' = 10^6\ M^{-1}\ s^{-1}$
reverse annealing	aDNA → ssDNA + primer	92−97	$k_a' = 100\ s^{-1}$
7-Reaction Model			
primer dimer complex	2(primer) → dimer	55−60	$k_{pd} = 5 \times 10^3\ M^{-1}\ s^{-1}$
dimer dissociation	dimer → 2(primer)	92−97	$k_{pd}' = 10^4\ s^{-1}$

were pipetted inside and the top surface sealed with another layer of tape. The reactors were then sandwiched between the preheated hot (95 °C) and cold (58 °C) plates of the convective device. After incubation for a desired time, the reactors were removed and the products were pipetted out of the wells for subsequent analysis by agarose gel electrophoresis (2 wt % gel (catalog no. 161-3107; Bio-Rad) with 1× TAE running buffer (catalog no. 141-0743; Bio-Rad)). Fluorescently stained DNA samples were prepared containing 2 μL of 100× SYBR Green I solution (Invitrogen/Molecular Probes), 2 μL of DNA sample, 2 μL of 6× Orange Loading Dye (Fermentas), and 4 μL of TAE buffer. Samples were run at 60 V for 1 h with a 100 bp DNA ladder sizing marker (catalog no. 170-8202; Bio-Rad).

A 3-D computational flow model was formulated to simulate the Rayleigh Bénard convective flow fields inside the microfluidic cylindrical cells. Geometries were created and meshed in Gambit (nonuniform hexahedral grids) and grid independence of solutions was verified. A finite volume solver (STAR-CCM+, CD-adapco) was used to simultaneously evaluate the continuity equation, 3D Navier−Stokes equations, and the energy conservation equation with the Boussinesq approximation in consideration of the buoyancy driven forces. Constant temperature boundary conditions were imposed on the top and bottom surfaces of the reactor (bottom = 97 °C and top = 53 °C), and the sidewalls were assumed to be thermally insulating with no slip and no penetration ($u = 0$) boundary conditions. Water was used as the fluid with its properties evaluated at the average temperature of the top and bottom surfaces. Both steady-state and transient velocity and temperature fields were obtained and further analyzed in Tecplot and MATLAB. For the reaction kinetic model, the species transport equation was solved with the coupled transient flow equations to obtain the time-resolved evolution of individual reagent concentrations (Supplementary Methods in the Supporting Information).

RESULTS AND DISCUSSION

Chaotic Flow Field. We formulated a 3D computational fluid dynamics (CFD) model to simulate the Lagrangian temperature versus time history experienced by an ensemble of over 300 randomly selected passive tracer trajectories during 5 min of convective PCR in cylindrical reactors of varying aspect ratio (h/d; here d was held constant at 1.5 mm). DNA replication occurs when reagents are sequentially transported through temperature zones associated with each stage of the reaction (e.g., denaturation, annealing, and extension), and occupy each zone for a sufficient residence time. Our simulations reveal that reagents occupy the extension zone, the rate limiting step in PCR, for a longer time in tall narrow reactors where the flow is laminar (e.g., $h/d = 9$), whereas a higher frequency of entry is observed in wider geometries where chaotic advection predominates (e.g., $h/d = 3$) (Figure 2a). Between these extremes, ensemble averages of the residence time and frequency of entry decrease and increase, respectively, with increasing aspect ratio. Residence times in the annealing and denaturing zones are relatively independent of aspect ratio (Figure 2b,c), but the frequency of entry in both zones is higher in chaotic flows. These trends are also mirrored in geometric dependence of the averaged quantities.

A key parameter is the number of complete replication cycles occurring over the course of each Lagrangian trajectory (i.e., representing sequential transport through annealing, extension, and denaturing zones). A much broader distribution (up to 15 complete cycles) is obtained at $h/d = 3$, whereas no more than 5 complete cycles occur at $h/d = 9$ (Figure 2d). These observations can be attributed to the convective flow field's increasingly chaotic characteristics at low aspect ratios, in contrast to the quasi-periodic motion evident in taller geometries.[5] These chaotic effects are inherently three-dimensional and therefore cannot be fully captured by a simplified 2D view, as has been adopted in previous studies.[6,7] Although these previous 2D modeling efforts have provided valuable insights and ideas that lay much of the groundwork for our studies, ultimately the three-dimensionality of the flow field plays a critical role in governing the reaction (Figure 2e and Supplementary Note in the Supporting Information). The fundamental importance of these chaotic flow phenomena arises because they drive two competing factors that govern PCR efficiency: (1) high aspect ratio (laminar, quasi-periodic) geometries are favorable because they deliver longer residence times in the extension zone, but (2) low aspect ratios (chaotic flow) are also favorable because they provide a higher frequency of entry and greater capacity to actuate complete replication cycles.

Coupling with Reaction Kinetics. We next incorporated reaction kinetics into the flow model to better understand the interplay between these competing effects (Table 1). Our analysis is based on a simplified 3-reaction framework introduced by Dorfman et al.[6,7] involving denaturation of the double stranded DNA template (dsDNA) into two single stranded constituents (ssDNA) at ∼95 °C, annealing of target specific oligomers (primers) to each ssDNA strand at ∼50−60 °C to generate annealed complexes (aDNA), and enzyme catalyzed incorporation of nucleotide species at ∼72 °C to synthesize the complementary strand yielding a completed dsDNA copy. We also introduced further complexity by incorporating reversibility into the denaturing and annealing steps (5-reaction model) and by considering side reactions associated with primer-dimer formation (7-reaction model). Although a

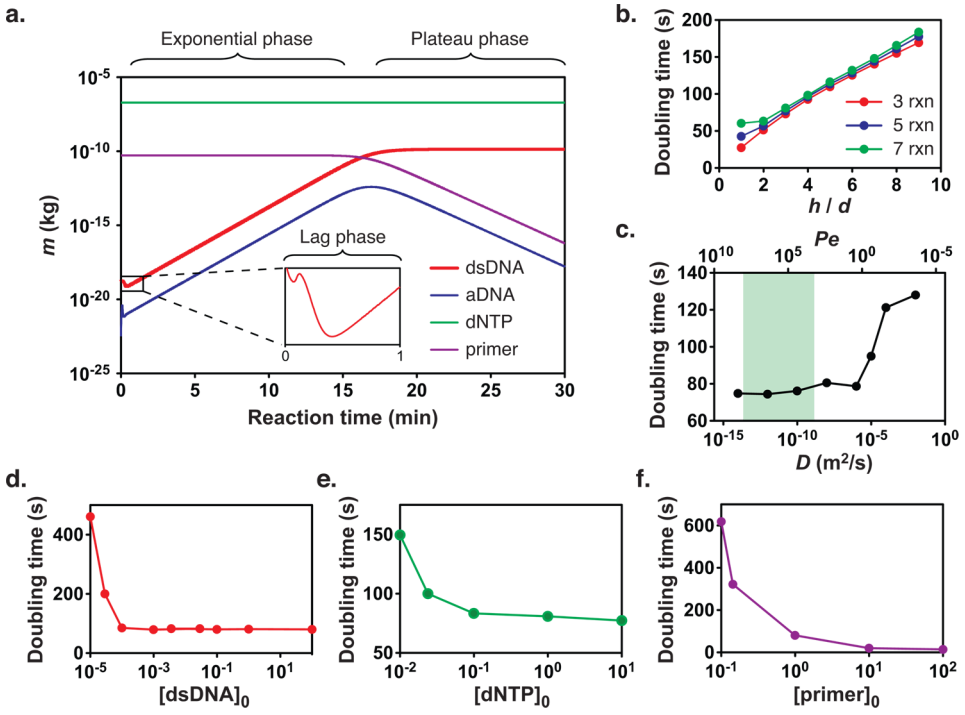

Figure 3. Coupled flow and reaction kinetics of convective DNA replication under thermal convection. (a) The time evolution of each species involved in a 3-reaction PCR model (Table 1) under chaotic flow conditions (h/d = 3) captures the characteristic lag, exponential, and plateau phases of DNA replication, resulting in a 10^9-fold increase in target yield over the initial template loading in less than 20 min. (b) Increasing the complexity of the reaction model by addition of side reactions (Table 1) does not appreciably impact the replication rate. (c) The variation of doubling time with DNA species diffusivity (lower ordinate) reveals a relatively constant replication rate over the full range of realistic parameter values (shaded region). Corresponding values of the Péclet number (upper abscissa) indicate that transport is convection-dominated in this regime. Replication rates are also computed as a function of initial concentrations (normalized with respect to their experimentally determined initial values) of (d) template DNA, (e) dNTPs, and (f) primers to establish optimal ranges for the convective format. All simulations were performed in the chaotic flow regime (h/d = 3).

complete description of PCR kinetics involves a complex network of multiple simultaneous processes (e.g., incomplete extension, polymerase deactivation, etc.), we focused our analysis on these simplified cases where rate constant data are readily obtainable.[8] Chemical reactions were formulated as part of a reaction-diffusion balance that was simultaneously solved with the transient flow profile to obtain the time-resolved evolution of individual species concentrations (Supplementary Methods in the Supporting Information).[3] Replication of a 250 bp dsDNA target was modeled, with the upper and lower surfaces of the cylindrical reactors held constant at 97 and 53 °C, respectively. Initial concentrations of individual species were selected based on conditions used in our previous experiments (Supplementary Methods in the Supporting Information). This model successfully captures the characteristic lag, exponential, and plateau phases of the PCR (Figure 3a). Briefly, the annealing rate is slower relative to denaturation in early stages of the PCR since the quantity of ssDNA is limited. This situation leads to an initial depletion in the dsDNA concentration (lag phase). Once a sufficient quantity of ssDNA accumulates, however, the annealing rate increases accompanied by a rapid increase in dsDNA concentration (exponential phase). Eventually exponential growth becomes inhibited again as the annealing rate decreases due to depletion of available primers (plateau phase).

In conventional PCR, the concept of a cycling time can be precisely defined because the reaction is executed uniformly throughout the bulk. Since this quantity is not straightforward to determine in the convective format due to the multiplicity of thermal trajectories present, we instead express the replication rate in terms of a characteristic doubling time. Comparing the effects of kinetic model complexity reveals that doubling times remain essentially unchanged in all geometries with an aspect ratio greater than 2 (Figure 3b). The slightly increased doubling time at very low aspect ratios when the 5 and 7 reaction models are applied likely reflects the reduced residence times available in these geometries (particularly in the extension zone) that would favor side reactions competing for ssDNA and thereby reduce the rate of target replication. Our simulations also reveal that target DNA diffusivity (a parameter that correlates with the target DNA length) does not appreciably impact the doubling time (Figure 3c). A more fundamental insight can also be obtained by expressing these results in terms of a dimensionless Péclet number (Pe) expressing the strength of convective transport relative to diffusive transport ($Pe = U\,d/D$, where U is the average flow velocity (1.67 mm/s; obtained by computing the average velocity magnitude in the reactor at h/d = 3), the length scale d is chosen to be the diameter of the cylindrical reactor (1.5 mm), and D is the DNA molecular diffusivity). Plotting the data in this way confirms that the flow is convection-dominated ($Pe \gg 1$) for realistic values of D, with the rapid increase in doubling time coinciding with conditions where $Pe \sim O(1)$. We next evaluated the effect of initial concentrations of template DNA, primers, and nucleotides (Figure 3d–f) which were normalized with their experimentally determined initial concentrations (Supplementary Methods in the Supporting Information). Increasing the amount of template DNA does not alter the doubling time, whereas kinetics

dx.doi.org/10.1021/ac402611s | Anal. Chem. 2013, 85, 10536–10541

are significantly slowed at normalized concentrations below 10^{-4} (i.e., the single copy limit, Supplementary Methods in the Supporting Information). Replication is also sensitive to the initial primer concentration, with a decrease in doubling time of 1−2 orders of magnitude (to less than 20 s) as the normalized concentration is increased. Likewise, the initial quantity of nucleotides in the reagent mixture does not significantly affect replication except at very low concentrations. Collectively, new insights make it possible to rationally select optimal reagent formulations to maximize the DNA replication rate.

Finally, we evaluated our reaction model across a wide range of *Ra* and h/d to establish a parametric mapping in terms of the generation rate, a quantity representing the number of target DNA doubling events per hour (i.e., the reciprocal of the doubling time). These results reveal that some of the most rapid generation rates are achieved in quasi-periodic laminar flow states immediately above the critical *Ra* associated with the onset of flow in the vicinity of $3 \geq h/d \geq 6$ (Figure 4, we

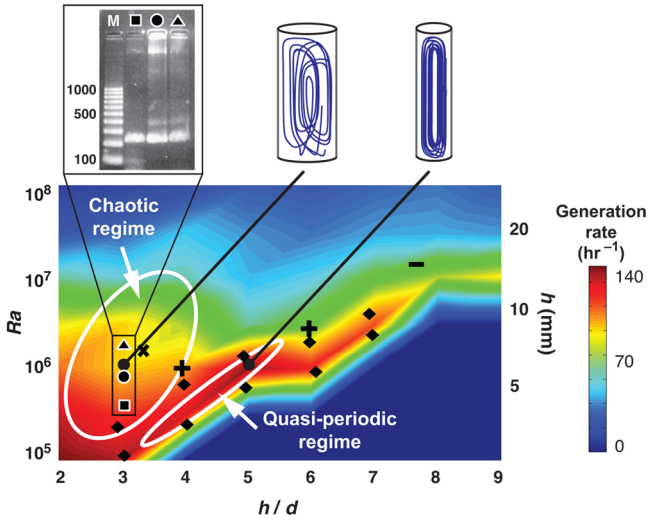

Figure 4. Microscale chaotic advection enables rapid DNA replication to be robustly achieved. Replication time scales expressed in terms of a generation rate (i.e., number of doubling events per hour) are simulated over a wide range of parameters. The parametric map reveals a zone in the chaotic flow regime where accelerated DNA replication is stably achievable over a span of 2 orders of magnitude in *Ra*, suggesting that reactors designed within this zone are capable of delivering consistent replication performance under virtually any combination of temperature and reactor volume associated with the PCR. Data points represent experimental results reported in the literature (see Table 2). Symbols in the gel electropherogram correspond to amplification of a 237 bp λ-phage DNA target in 12 min reported in this work using three different reactor geometries.

remark that the boundaries of these kinetic regimes are mispredicted by simplified 2D models (Supplementary Note in the Supporting Information)). These geometries have the smallest allowable height at a given aspect ratio, thereby enabling reagents to circulate quickly throughout the reactor. More significantly, a broad zone is evident within the central chaotic flow regime where generation rates remain essentially unchanged. Although replication is not quite as fast as in the vicinity of the critical *Ra*, reactions nevertheless proceed rapidly enough to execute the equivalent of a typical 30 cycle PCR in 10−20 min, consistent with our experimental results.[3] Remarkably, generation rates in the chaotic flow regime remain essentially constant over nearly 2 orders of magnitude of *Ra*, thereby encompassing virtually all possible combinations of temperature and reactor volume associated with realistic PCR conditions. We verified the robustness of PCR performed within the chaotic flow regime by amplifying a 237 bp fragment associated with λ-phage DNA in three different reactor geometries (h/d = 3, with h = 4.5, 6.0, and 7.5 mm). All reactions were allowed to run for 12 min. Successful amplification was achieved in all three geometries within this accelerated reaction time (Figure 4), consistent with the predicted generation rate in this regime. More broadly, our predictions are corroborated by results from previous studies involving PCR under Rayleigh Bénard convection summarized in Table 2 and indicated on the parametric map in Figure 4.

Table 2. Overview of Experiments Reported in Literature Involving PCR under Rayleigh-Bénard Convection

ref	replication target	reaction time (min)	symbol in Figure 4
Priye et al. (this work)	λ-phage DNA (237 bp)	12	■, ●, ▲
Priye et al.[4]	λ-phage DNA (237 bp)	10−20	+
Muddu et al.[3]	human β-actin gene (295 bp)	10	×
Yao et al.[9]	calf thymus DNA (407 bp)	8−17	♦
Chou et al.[10]	pHBV-48, HCV plasmid, HIV-1 vector pNL4-3 (122 to 222 bp)	10−30	−
Chang et al.[11]	yellow head virus (67 bp)	10−20	off scale (h/d = 11.6)
Krishnan et al.[2]	influenza A virus (191 bp), human β-actin gene (295 bp)	15−30	off scale (h/d > 9)
Ugaz et al.[12]	influenza A virus (191 bp), human β-actin gene (474 bp)	15−30	off scale (h/d > 9)
Krishnan et al.[1]	human β-actin gene (295 bp)	90	off scale (h/d = 10)

CONCLUSION

Our results reveal an incredibly robust regime where rapid DNA replication is achievable independent of specific reactor geometries and temperatures, addressing limitations that have been previously viewed as a major drawback of the convective thermocycling format. Because the convective flow field is inherently dependent on the geometric and thermal conditions imposed, it has been generally accepted that the versatility of convective PCR is limited because reactor geometries would need to be specifically matched to the biochemical requirements of individual reactions. Our kinetic mapping contradicts this view, suggesting instead that a properly designed standard reactor geometry within the chaotic flow regime can be universally functional (e.g., analogous to conventional PCR tubes).

ASSOCIATED CONTENT

Supporting Information

Additional information as noted in text. This material is available free of charge via the Internet at http://pubs.acs.org.

AUTHOR INFORMATION

Corresponding Author

*Phone: +1 979-458-1002. Fax: +1 979-845-6446. E-mail: ugaz@tamu.edu.

Notes

The authors declare no competing financial interest.

■ ACKNOWLEDGMENTS

This work was supported in part by the U.S. National Science Foundation (NSF) under Grant CBET-1034002. We thank Mr. Kyle Palmer, supported by an NSF Research Experience for Undergraduates (REU) program, for assistance and helpful discussions with the kinetic model formulation.

■ REFERENCES

(1) Krishnan, M.; Ugaz, V. M.; Burns, M. A. *Science* **2002**, *298*, 793−793.
(2) Krishnan, M.; Agrawal, N.; Burns, M. A.; Ugaz, V. M. *Anal. Chem.* **2004**, *76*, 6254−6265.
(3) Muddu, R.; Hassan, Y. A.; Ugaz, V. M. *Angew. Chem., Int. Ed.* **2011**, *50*, 3048−3052.
(4) Priye, A.; Hassan, Y. A.; Ugaz, V. M. *Lab Chip* **2012**, *12*, 4946−4954.
(5) Muddu, R.; Hassan, Y. A.; Ugaz, V. M. *J. Vis. Exp.* **2011**, *49*, e2366.
(6) Yariv, E.; Ben-Dov, G.; Dorfman, K. D. *Europhys. Lett.* **2005**, *71*, 1008−1014.
(7) Allen, J. W.; Kenward, M.; Dorfman, K. D. *Microfluid. Nanofluid.* **2009**, *6*, 121−130.
(8) Mehra, S.; Hu, W. S. *Biotechnol. Bioeng.* **2005**, *91*, 848−860.
(9) Yao, D.-J.; Chen, J.-R.; Ju, W.-T. *J. Micro-Nanolith. MEMS MOEMS* **2007**, *6*, 043007−043007−9.
(10) Chou, W. P.; Chen, P. H., Jr; Miao, M.; Kuo, L. S.; Yeh, S. H.; Chen, P. J. *Biotechniques* **2011**, *50*, 52.
(11) Chang, H. F. G.; Tsai, Y. L.; Tsai, C. F.; Lin, C. K.; Lee, P. Y.; Teng, P. H.; Su, C.; Jeng, C. C. *Biotechnol. J.* **2012**, *7*, 662−666.
(12) Ugaz, V. M.; Krishnan, M. *J. Lab. Autom.* **2004**, *9*, 318−323.